npj Computational Materials

www.nature.com/npjcompumats

ARTICLE OPEN

Distortion-stabilized ordered structures in $A_2BB'O_7$ mixed pyrochlores

Ghanshyam Pilania[1], Brian Puchala[2] and Blas P. Uberuaga[1]

Pyrochlore oxides ($A_2B_2O_7$) are interesting for a number of technological applications, including radiation damage tolerance and as ionic conductors. Mixed pyrochlores—containing two A and/or two B site cations—provide even more flexibility for tailoring properties owing to the diverse chemical and configurational degrees of freedom accessible within this chemical space. Here, we examine relative stability of different cation orderings in one model double pyrochlore $Gd_2(Zr_xTi_{1-x})_2O_7$, as a function of Zr content x. Our results show that, in the presence of some very specific local cation arrangements, certain cation-ordered compositions in this system are highly stabilized as a result of large oxygen relaxation displacements, leading to the formation of an ordered 'double' pyrochlore structure. The origins of these anomalous oxygen relaxations are traced back to both the local cation symmetry and a strong chemical preference of Zr atoms towards adopting a 7-fold coordination environment, as opposed to a 6-fold coordination available in a regular pyrochlore structure. Subsequently, we examine the stability of this type of ordering in 131 other pyrochlore compositions. Implications of our findings are discussed in relation to the observed composition-dependent ionic conductivity in these systems and connections with previously reported experimental findings are made.

npj Computational Materials (2019)5:7 ; https://doi.org/10.1038/s41524-018-0144-1

INTRODUCTION

Oxides are an attractive class of materials due to their extreme variety in functionality. This richness arises from the very flexible chemistry of these materials. Indeed, beyond base compounds such as binaries and ternaries, the possibilities for modifying the chemistry of most oxides is nearly limitless. Such multicomponent oxides often have significantly improved performance over the end-member compounds, with enhanced scintillation,[1] ferroelectricity,[2,3] piezoelectricity,[4] high temperature stability[5] and catalytic response.[6] By expanding the chemical space in which compound discovery can occur by considering mixed oxides, the potential for materials discovery expands exponentially.

Thus, in the quest for new materials, understanding the structures that result from mixing simpler compounds to form more complex materials is critical. This has been extensively studied in some cases. For example, in the perovskite family of compounds (ABO_3), the properties of so-called double perovskites have been examined by multiple groups.[7,8] These compounds, containing two A and/or two B cations, can form ordered structures for some chemistries[9–11] and these orderings are known to modify functional properties, including oxygen transport[12,13] and ferromagnetism.[14]

In the case of pyrochlores ($A_2B_2O_7$), the subject of the current work, mixed systems have been used to understand, amongst other properties, the role of disorder in both radiation damage tolerance and ionic conductivity. Simply, as, for example, the B cation is gradually changed from Ti and Zr, the propensity for cation disorder increases and this has been correlated to the functionality of the material. In materials such as $Gd_2(Zr_xTi_{1-x})_2O_7$ (GZTO), as the chemistry shifts from $x = 0$ to $x = 1$, disorder increases and so does the resistance to amorphization[15–17] and the magnitude of ionic conductivity.[18] Thus, in many studies of ionic conductivity, disorder is induced in the system via the introduction of additional cations.[18–20] These studies have led to conflicting results, with some showing a direct increase in the conductivity vs. disorder[18] while others suggest that the ordered phase has a higher conductivity than the disordered state.[19,20]

Implicitly, these studies assume a smooth and gradual transition from the ordered state to the disordered state with changes in chemistry. However, this is not always the case. For example, NMR studies show that, depending on both the A and B chemistry of the compound, mixed pyrochlores can form either solid solutions or phase separate.[21,22] This complicates the establishment of structure-property relationships with disorder.

In this work, we consider a further complication, the possibility that, even in cases where the cations form a solid solution in mixed pyrochlores, they may form ordered structures, reminiscent of the double perovskites, rather than a disordered solid solution. These ordered structures would naturally exhibit different transport behavior than a random solid solution, as we have seen previously for double perovskites.[13] Thus, in any campaign to establish structure-property relationships for mixed pyrochlores, one must have a solid understanding of what the detailed atomic structure of the mixed pyrochlore is. We use density functional theory (DFT) to investigate the possible orderings as a function of x in $Gd_2(Zr_xTi_{1-x})_2O_7$. We identify unique ordered ground states that are stabilized by significant distortions in the oxygen sublattice, distortions that increase the coordination of Zr from 6 to 7. We then examine the stability of this ordering in other pyrochlore compositions. We find that in many compositions in which the A cation is of sufficient size and the B sublattice contains sufficient Zr and/or Hf, ordered structures are

[1]Materials Science and Technology Division, Los Alamos National Laboratory, Los Alamos, NM 87545, USA and [2]Materials Science and Engineering Department, University of Michigan, Ann Arbor, MI 48109, USA
Correspondence: Ghanshyam Pilania (gpilania@lanl.gov) or Blas P. Uberuaga (blas@lanl.gov)

Received: 23 July 2018 Accepted: 12 December 2018
Published online: 14 January 2019

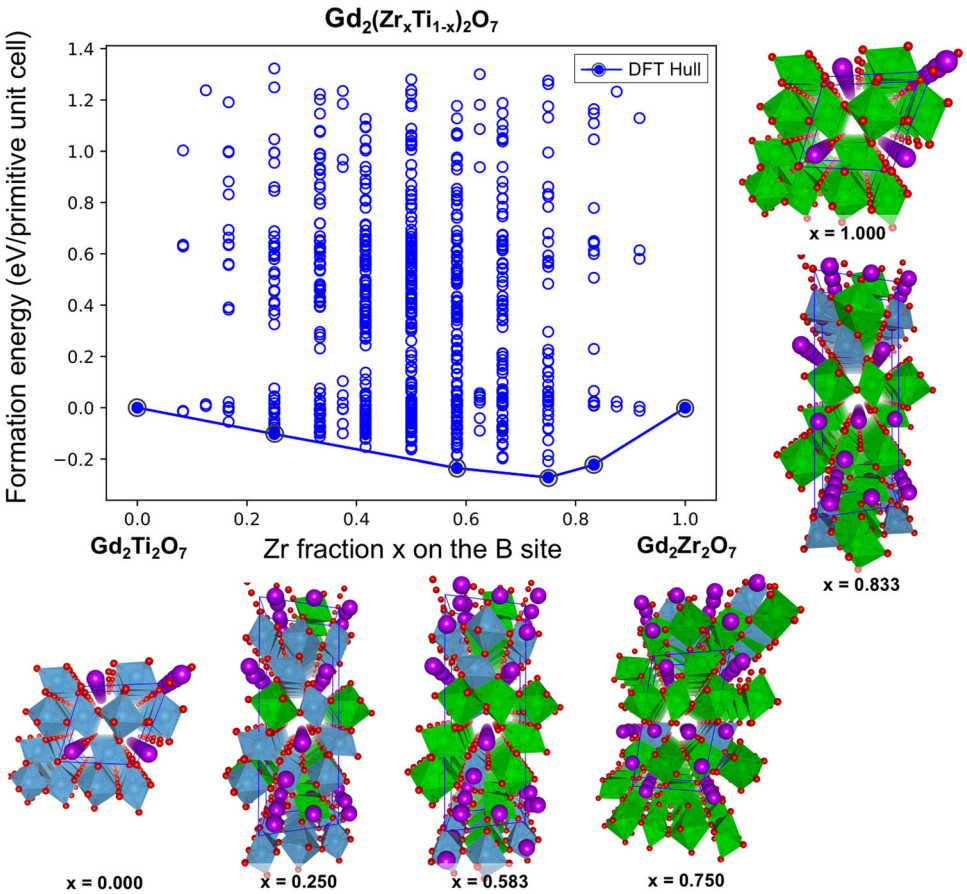

Fig. 1 Calculated mixing energies (*i.e.*, formation energies relative to the pure single pyrochlore end point compositions with $x = 0$ and $x = 1$) per primitive unit cell (with 22 atoms, containing two effective pyrochlore formula units) for the entire set of 704 unique configurations enumerated within the $Gd_2(Zr_xTi_{1-x})_2O_7$ chemistries. The DFT predicted convex hull is represented as a solid line. The atomistic structures for the identified ground-state ordered structures on the convex hull are illustrated. While Gd and O atoms are represented by purple and red spheres, Ti and Zr polyhedra are depicted in blue and green colors, respectively

thermodynamically preferred, at least at low temperature. These results offer new insight into the structures that drive performance in mixed pyrochlores.

RESULTS

The DFT-computed mixing energies (*i.e.*, the formation energies with respect to the pure pyrochlore chemistries with $x = 0$ and $x = 1$) for the entire set of 704 configurations enumerated within the generalized $Gd_2(Zr_xTi_{1-x})_2O_7$ formula unit are presented in Fig. 1. In addition to the end points, the DFT-computed convex hull identifies four different ground-state structures with compositions $x = 0.25$, 0.583, 0.75 and 0.833 (the relaxed geometries are provided in the Supporting Information). The atomistic structures for the identified ground-state ordered structures are also depicted in Fig. 1. The DFT results in Fig. 1 indicate that, as the composition varies from Ti rich to Zr rich, there are ordered structures of Ti and Zr on the B-sublattice that are thermodynamically stable. Thus, similar to double perovskites, these mixed pyrochlore systems may also exhibit some tendency to form ordered solid solutions. Further, the propensity for ordering is greatest for a Zr-rich composition of $x = 0.75$, indicating that the propensity for forming an ordered structure is sensitive to the composition of the mixed system.

We further note that the specific orderings identified in Fig. 1 between $x = 0$ and $x = 1$ (*i.e.*, mixed pyrochlores) all have a superstructure that is longer-ranged than simple "single" pyrochlore structure. In other words, the orderings are not possible with

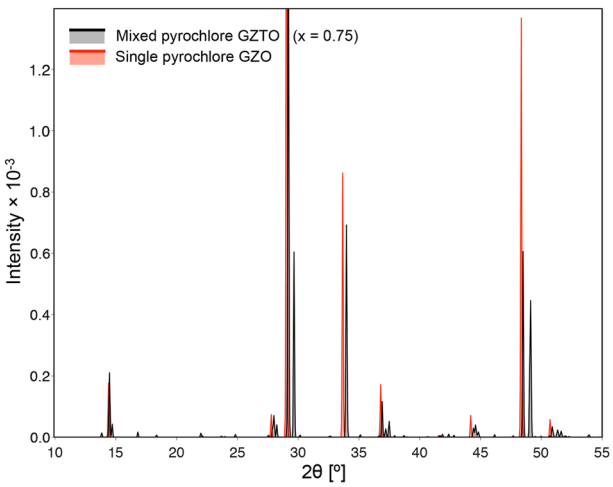

Fig. 2 Simulated XRD patterns for mixed GZTO, using the DFT-computed ground-state structure with $x = 0.75$ (black), and GZO (red) pyrochlores. CrystalDiffract was used to simulate the theoretical XRD patterns from the pyrochlore supercell geometries[43] and an orthogonalized supercell was used for simulating the XRD spectra[44]

the standard pyrochlore primitive unit cell containing 22 atoms (i.e., two formula units) and need either 44-atom (for $x = 0.75$) or 66-atom supercells (for $x = 0.25$, 0.583, and 0.833). To look for specific signatures for the aforementioned cation ordering, in Fig. 2

we compare the X-ray diffraction (XRD) patterns for mixed GZTO (using the DFT-computed ground-state structure with $x = 0.75$ that exhibits the lowest mixing energy) and GZO pyrochlores. It can be seen that as a consequence of B-site ordering some of the peaks in the "single" pyrochlore GZO are split in the mixed GZTO structure. Furthermore, we also find some new (weak) peaks at various angles that are a reflection of the ordering in the mixed structure.

The DFT calculations provide the zero-Kelvin ground-state structure and a range of higher-energy metastable structures for each composition. Thus, while the ground states are ordered structures, it is possible that their range of stability versus temperature is rather limited. One approach to understand the temperature-dependent phase stability of these structures is to use Monte Carlo. Given the expense of doing Monte Carlo directly with DFT energetics, we turn to CE to parameterize an effective Hamiltonian.

As a next step, we use the DFT computations to fit a CE Hamiltonian to describe energetics of any given atomic configuration and composition x for the B-site ordered pyrochlore chemistries. We included the entire set of 704 configurations in the CE fitting while closely following the approach previously described.[23] During the effective cluster interactions (ECI) optimization procedure, we systematically considered clusters with up to n-body interactions with $n \in [4, 7]$ while gradually varying the maximum allowed site spacing between the n-body clusters from 7 Å to 10 Å. Our CE analysis showed that while CE fits with small and moderate basis sets failed to describe the DFT grounds states, ECIs chosen from a much larger set (with up to 7-body interactions and maximum allowed site spacing of 10 Å) were able to adequately capture the relative energetics of the structures in the CE training set (see Fig. S1 in the Supporting Information). Although the adopted ECI optimization procedure explicitly included a k-fold cross-validation strategy to select the best set of ECIs (in order to avoid overfitting to the training data and thereby leading to a better generalizability on unseen configurations), we found that the unusually large basis sets that were eventually able to provide a good fit for the entire set of low-energy DFT configurations inevitably led to an overfitting of the training data.

To further understand the poor performance of the CE fits to the DFT-computed energetics, we looked into basis and lattice relaxation patterns of the DFT configurations used in the fitting procedure. Our analysis identifies large basis deformations for a subset of the compounds as a cause of this problem. More specifically, we find that in certain local chemical environments O atoms display unusually large relaxation displacements (~1.5 Å), which not only lower the energies and volumes of the supercells significantly, but also result in local coordination environment changes of the nearby cations. Essentially, a subset of oxygen atoms displace away from their initial pyrochlore lattice positions, forming a structure that does not correspond exactly to that of pyrochlore. Such relaxations have not been previously reported for any pyrochlore chemistries, to the best of our knowledge.

In order to quantify the extent of the basis deformations resulting from the anomalous O relaxations, we define a cost function that describes the degree to which basis sites have relaxed with respect to the ideal pyrochlore structure. The basis deformation cost function is defined as the mean squared displacement of atoms from their position in the relaxed ideal structure (i.e., a reference structure accounting for the lattice relaxations but the internal coordinates fixed to the unrelaxed ideal positions). Figure 3a, b present formation energies and volumes of the relaxed structures per 22 atom primitive cell as a function of composition, with the marker colors representing the extent of the basis deformation. It is interesting to note that while ground-state compounds with $x < 0.5$ (i.e., the Ti-rich chemistries) exhibit only minimal relaxations with respect to the ideal pyrochlore configuration, the ground states with Zr-rich chemistries consistently show a significant amount of basis deformation. Furthermore, these local relaxations also result in a lowering of the overall volume of the supercells. This can be seen from Fig. 3b, where mixing of the two pyrochlore chemistries, in general, leads to configurations that show either equal or larger volumes with respect to what is expected from a simple linear interpolation, but those configurations showing relatively large basis deformations clearly stand out with significantly lower supercell volumes.

To illustrate the nature of the local O relaxations, we take the specific example of the $x = 0.75$ ground-state configuration. Figure 3c, d present the unrelaxed and DFT-relaxed supercell geometries, respectively, for this ground-state structure. The relaxation amplitudes and directions of the O atoms that are largely responsible for the large basis deformation are identified with black arrows in Fig. 3c. It can be seen that as a result of the relaxation, O atoms common to the two Ti octahedra move significantly closer to a nearby Zr octahedron. As a result, the coordination environment of the Zr atom changes from 6-fold to 7-fold, while the two Ti atoms remain 6-fold coordinated, albeit with slightly distorted octahedra, as shown in Fig. 3e. Our analysis shows that as a general requirement for the aforementioned large O relaxations to occur, the following two conditions have to be met: (1) an O atom must be common to the two corner sharing Ti octahedra and (2) a nearby Zr atom must have an asymmetric local atomic environment of surrounding cations. As an example, to illustrate the second condition, Fig. 3f–g depict two representative cases from our DFT-computed dataset where the first condition is met for both structures, however, owing to the local symmetry breaking, only the Zr atoms in the supercell shown in Fig. 3g can relax to a 7-fold coordinated environment. Note that the symmetry argument made above also explains why the pure $x = 1$ case (i.e., the $Gd_2Zr_2O_7$ single pyrochlore) does not exhibit such O distortions, although Zr atoms favor a 7-fold coordination.

To further understand the O relaxations in the context of well established notions of the "kagome" pattern formed by oxygen in single pyrochlores,[24,25] we take a look at the collective patterns of atoms in a oxygen–metal–oxygen layer stacking normal to the [111] direction corresponding to a pseudo-cubic pyrochlore supercell, as shown in Fig. 4a. We note here that the pyrochlore (with stoichiometry M_4O_7, without differentiating the two different metal ions M) structure is fundamentally related to a parent fluorite (MO_2) structure. Owing to the different metal–oxygen stoichiometry, however, the individual structure of oxygen atoms in each layer in the two structures differs. More specifically, pyrochlore differs from fluorite in that half of the oxygen planes contain structural vacancies that form a "kagome" pattern and have the extra complexity of having two different cationic species.

In Fig. 4, we compare the local O relaxation patterns in relaxed $Gd_2(Zr_{0.75}Ti_{0.25})_2O_7$ (Fig. 4d, e) with the corresponding bulk-like single pyrochlore structure (Fig. 4b, c). For easy comparison, we show three stacked oxygen–metal–oxygen layers (side view shown in Fig. 4a and also identified in the central panel) where the central metal layer contains only Gd and Ti cations and the oxygen layer directly above the metal layer contains O atoms that exhibit the predicted anomalous relaxations. While oxygen atoms in both the top and the bottom layers are visible in Fig. 4b, d, only top layer oxygen atoms are shown in Fig. 4c, e, and the "kagome" pattern formed by oxygen atoms in the top layer is highlighted in selected panels as a guide to the eye. From Fig. 4a–e, it can be seen that as a result of the O relaxations of selected O atoms in the top layer (identified by black arrows in the right panels) alternate triangles in the "kagome" pattern" are affected as the O atoms relax from the vertices to the near-centroid positions.

A physically meaningful CE fit can still be possible in the presence of a limited set of training configurations that lead to large basis deformations upon relaxation, provided the resulting

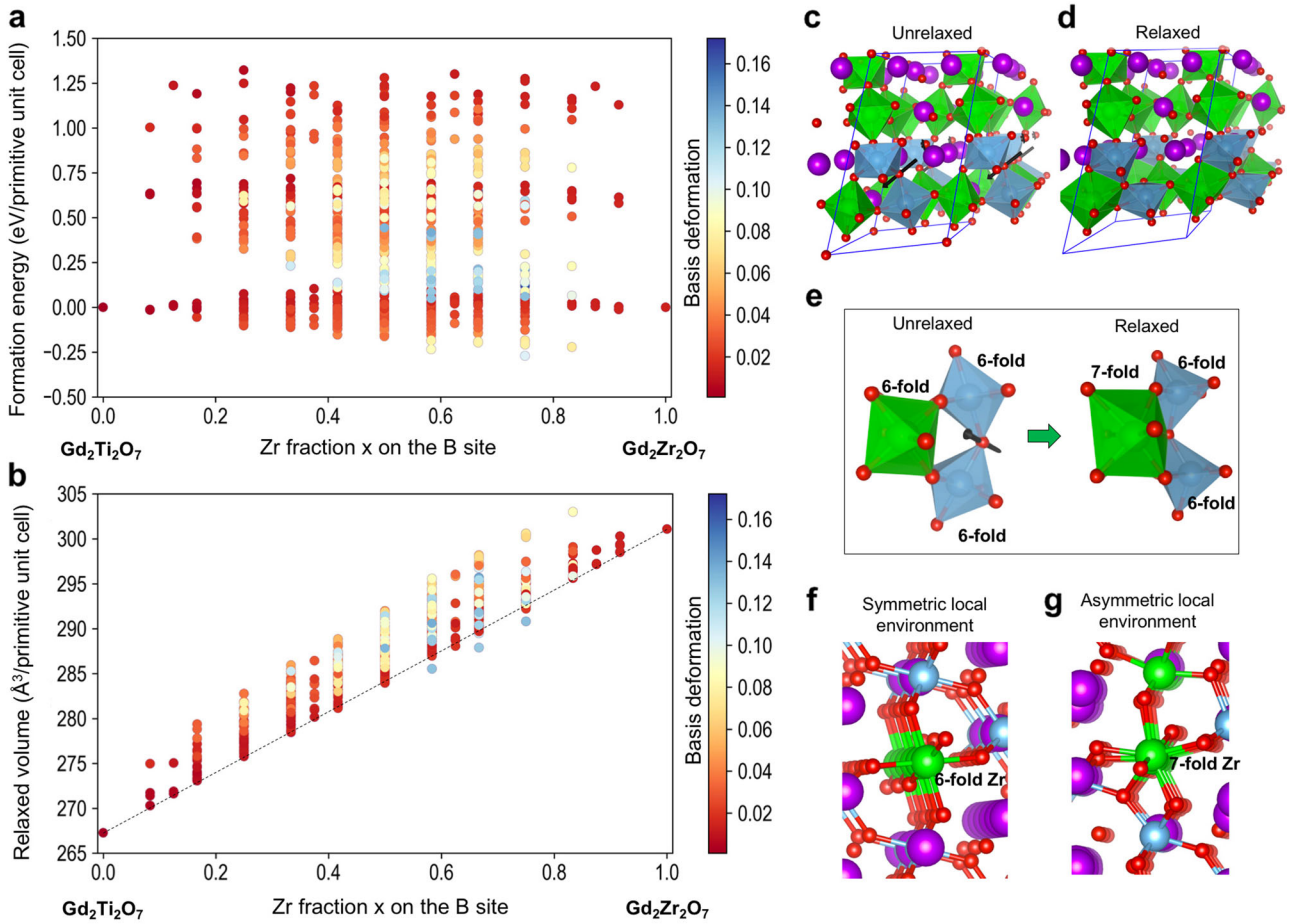

Fig. 3 **a** Basis deformation mapped DFT-computed mixing energies and **b** relaxed volumes (normalized to a primitive cell containing 22 atoms, *i.e.*, 2 effective pyrochlore formula units) as a function of composition. The colors represent the extent of the basis deformation. The dashed line in **b** represents a Vegard's law based interpolation. **c**, **d** Unrelaxed and DFT-relaxed supercell geometries for the $Gd_2(Zr_{0.75}Ti_{0.25})_2O_7$ ground-state structure. The relaxation of O atoms that are largely responsible for the large basis deformation are identified with black arrows (these structures are the same as shown in Fig. 1, just a different perspective and with fewer periodic images). **e** A closer view of the coordination environment changes as a result of the large O relaxations for the ground-state configuration. The coordination environment of the Zr atom changes from 6-fold to 7-fold, while the two Ti atoms remain 6-fold coordinated, although with slightly distorted octahedra. **f**, **g** Two representative cases from the DFT-computed dataset where local symmetry breaking around the Zr atoms drives the predicted large O relaxation behavior. When this symmetry breaking does not occur (as in f), the O atoms do not relax so significantly

structures are sufficiently higher in energy with respect to the ground-state structures and therefore minimally contribute to the determination of lower regions of the potential energy surfaces. In such a situation, omitting these structures from the training dataset used in the CE fitting generally improves the quality of the resulting fits, without sacrificing the underlying "physics" of the problem. However, in the present case, a large fraction of the identified ground-state chemistries (i.e., all the mixed Zr-rich cases) exhibit large basis deformations and therefore an effective Hamiltonian obtained by refitting a CE model after removing the structures that exhibit anomalously large O relaxations will not be a very realistic one. The inability to fit a CE Hamiltonian for the $Gd_2(Zr_xTi_{1-x})_2O_7$ mixed pyrochlore system within the scope of this work prevents us from examining the thermal phase diagram and determining the stability field for the ordered structures. While this is a negative result, our DFT-based results clearly show that certain ordered mixed pyrochlore chemistries are indeed thermodynamically favorable—with a strong theoretical evidence that the local chemical environments in such mixed or *double* pyrochlores may significantly deviate from their *single* pyrochlore bulk counterparts.

The results presented thus far naturally lead to the following question: "How general are these findings?" To address this question as to whether the theoretical findings are specific to the $Gd_2(Zr_xTi_{1-x})_2O_7$ mixed pyrochlore system or represent the behavior of a much wider class of chemistries, we next explore chemical trends within a set of 132 different mixed pyrochlore chemistries of $A_2(B_{0.25}B'_{0.75})_2O_7$-type. The details of the specific choices considered for A, B and B′ chemistries are provided in the Methods section, towards the end of the manuscript. An analysis identical to that for $Gd_2(Zr_xTi_{1-x})_2O_7$ across this entire chemical space would require DFT-computations of 704 compounds for each of these chemistries—beyond the scope of the present study. Therefore, the mixed pyrochlores are simulated using the supercell configuration that exhibits the lowest mixing enthalpies for the $Gd_2(Zr_xTi_{1-x})_2O_7$ system. We note that the specific ordering we have chosen to study relative trends across different chemistries may not represent ground-state configurations for the respective chemistries, but mixing energies computed with this ordering certainly constitute an upper bound on the minimum energy of mixing for the corresponding $A_2(B_{0.25}B'_{0.75})_2O_7$-type double pyrochlores. More importantly, using this structure and the associated cation ordering for the target chemical space exploration allows for O relaxations that are responsible for Zr coordination switching from a 6-fold to a 7-fold environment upon relaxation in $Gd_2(Zr_{0.75}Ti_{0.25})_2O_7$ with a large

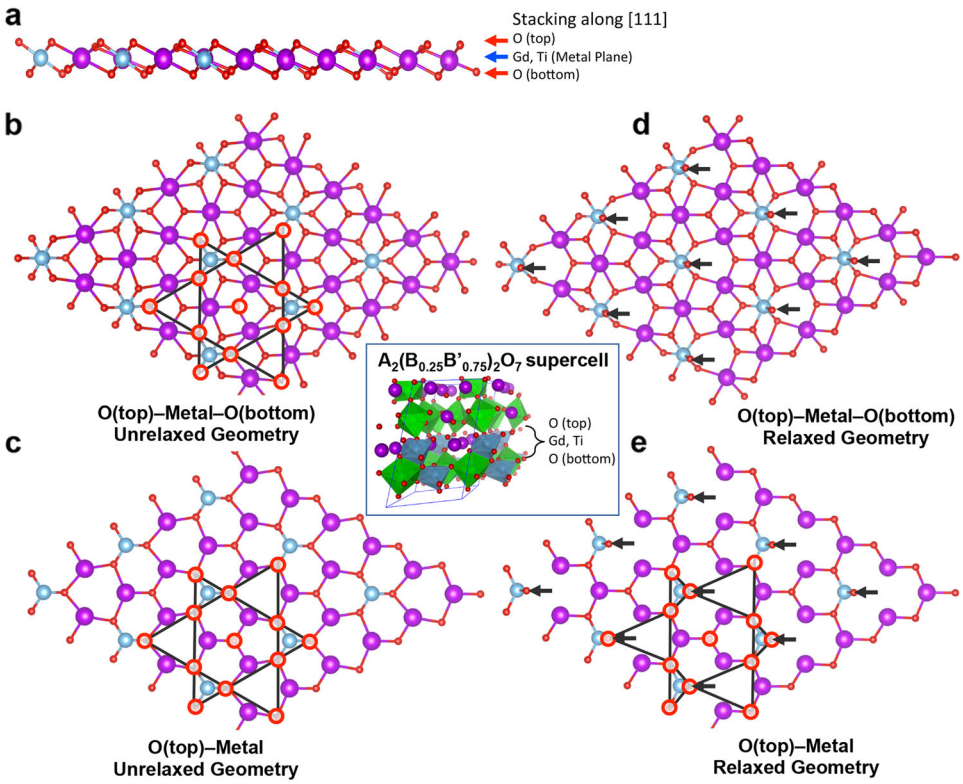

Fig. 4 Visualization of collective pattern of the anomalously large O relaxations in the context of the well known "kagome" pattern of O atoms in the $Gd_2(Zr_{0.75}Ti_{0.25})_2O_7$ ground-state structure. While **a** shows the side view of the selected oxygen–metal–oxygen layers, **b**, **c** and **d**,**e** respectively compare the unrelaxed and DFT-relaxed top views for the same. While **b**, **d** show O atoms in both the top and the bottom layers, for clarity, O atoms only in the top layer are visible in **c**, **e**. The center panel identifies the three specific layers in the supercell shown in Fig. 3d, which are used here to visualize the relaxation pattern of O atoms. The most prominent O relaxations are identified with black arrows and the "kagome" pattern formed by O atoms in the top O layer is highlighted in selected panels

energetic contribution to the mixing energy. Thus, this also allows us to gain further insight into the chemical driver of the large O relaxation.

Figure 5a presents results of our DFT-computed mixing energies for the aforementioned 132 $A_2(B_{0.25}B'_{0.75})_2O_7$ double pyrochlores. The chemistries are grouped according to the A-site chemistries in different panels, which are presented in decreasing order of the A elemental empirical radii going from A = La to A = Lu.[26] For a given A-site chemistry, B and B' chemistries are identified along the vertical and horizontal axis, respectively. Several interesting observations can be made from the results presented in Fig. 5a. Most remarkably, the mixing energy patterns in different panels can be visually classified in to two different classes. The chemistries with A ∈{La, Pr, Nd, Sm} appear to behave qualitatively different from the rest. A deeper case-by-case analysis reveals that within this set of compounds the aforementioned O relaxation displacements are not energetically favorable, irrespective of the B and B′ chemistries.

In contrast, for the double pyrochlore chemistries with A ∈{Y, Gd, Tb, Dy, Ho, Er, Lu}, a number of B and B' chemistries exhibit the energetically favorable mixing driven largely by the O relaxation displacements, similar to those identified in Fig. 3 for $Gd_2(Ti_{0.25}Zr_{0.75})_2O_7$. In particular, the double pyrochlore chemistries with Zr and Hf atoms at the B′ site generally show both favorable mixing tendencies as well as the anomalous O relaxation displacements. To further establish the fact that the chemical trends in mixing energies within this subset of compounds are indeed largely dictated by the O relaxation displacements, in Fig. 5b we present the energy contributions due to O relaxation displacements to the total mixing energies (*cf.* Fig. S2 in the Supporting Information for the associated supercell volume changes). In each case, the relaxation energies are computed by comparing the energetics of a completely relaxed structure with the one where all internal coordinates are allowed to relax except the O atom that exhibits anomalous relaxation displacement (*cf.* Fig. 3e). This is practically carried out by restricting the relaxation displacements of the O atom as well as the nearby B′ site atom whose coordination is altered after the relaxation (note that just restricting the relaxation of the O atoms internal coordinates would not be sufficient, as the rest of the supercell atoms can then relax relative to the O atom). Figure 5b clearly demonstrates that the mixing energy trends in this set of compounds are indeed largely governed by the relaxation displacements of the O atom. That is, the most stable of the mixed compounds in Fig. 5a correspond to those in which allowing the O relaxation to occur results in the biggest lowering of energy in Fig. 5b.

Most interestingly, Fig. 5a points to other compositions in which the propensity of ordering of the mixed phases might be even higher than in $Gd_2(Zr_xTi_{1-x})_2O_7$. For example within the A = Gd system, a composition of 75% Zr and 25% Hf exhibits significantly stronger ordering tendencies. There are also strongly ordered pairings in the A = Ho, Er, and La families of compounds, many involving mixings of Zr and Hf, but some combinations with Ti and even Sn are relatively stable. Thus, in experimental searches for ordered mixed pyrochlores, some of these compositions may prove more fruitful.

Conversely, compounds involving mixing Sn and Ti on the B sublattice are almost universally unfavorable, at least with the ordered structure used here. There have been multiple studies, several using NMR, to examine mixed pyrochlores containing Sn. In the case of Sn and Ti pairings, if the A cation was Y, the system formed a solid solution[21] while, when A = La, the system tended

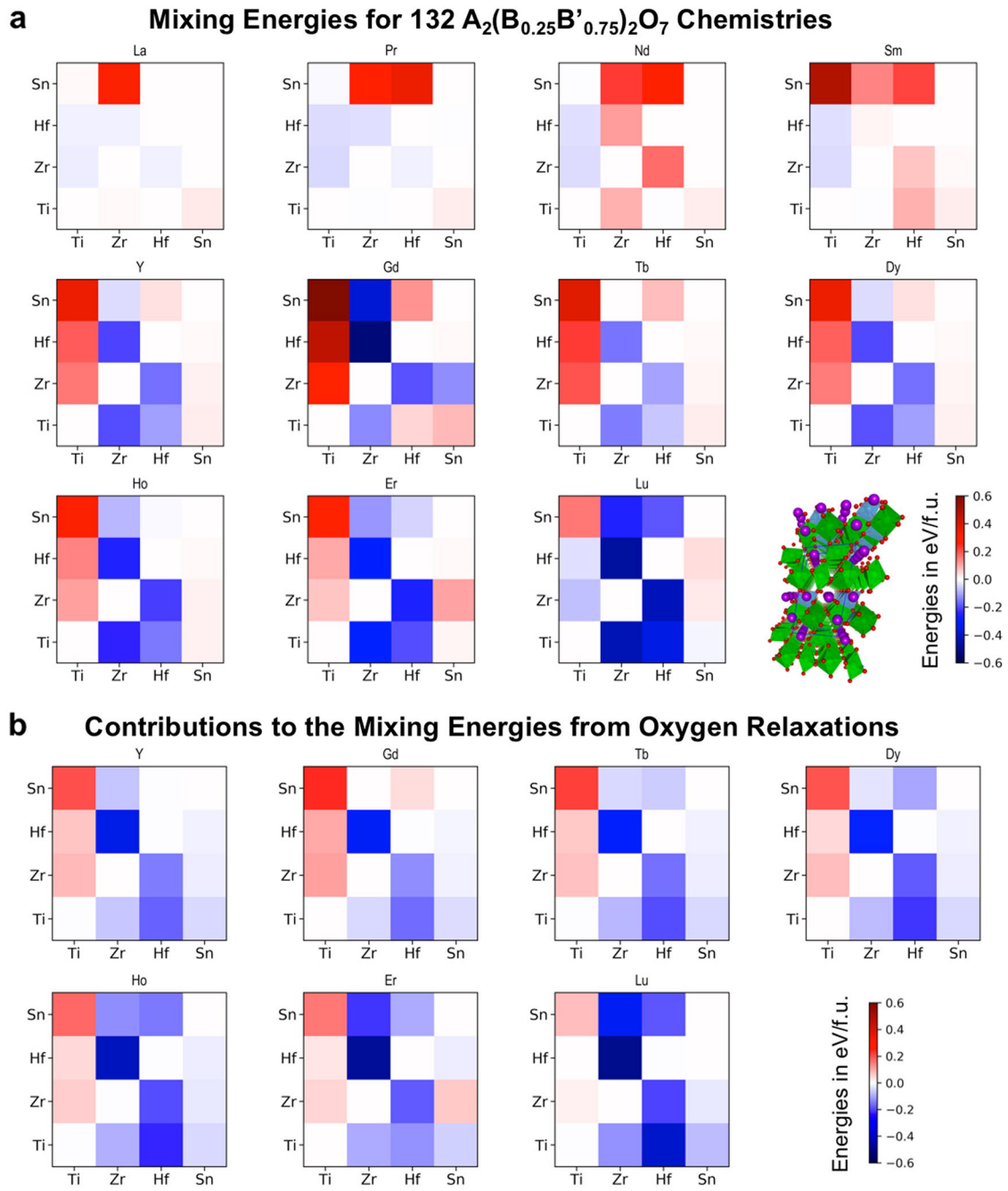

Fig. 5 **a** DFT-computed mixing energies per formula unit for a set of 132 $A_2(B_{0.25}B'_{0.75})_2O_7$ double pyrochlores. The chemistries are grouped according to the A-site chemistries identified on the top of the each panel. Labels on the vertical and horizontal axis identify B and B′ chemistries, respectively. The $Gd_2(Zr_{0.75}Ti_{0.25})_2O_7$ ground-state structure employed in the DFT energetics computations is also shown in the bottom right panel. **b** For a selected set of A-site chemistries (that exhibit the identified large O-relaxation), mixing energy contributions arising purely due to the aforementioned O relaxations are presented. Note that the relative energetics presented in **b** closely follows the pattern in **a** when comparing the respective chemistries, indicating that the trends in the mixing energetics are indeed largely governed by the O relaxation energetics

to phase separate or even from a perovskite phase.[22] Our results are not directly comparable to these experiments as our calculations are at 0 K and we are unable, because of the lack of a suitable CE, to examine the finite temperature behavior of the mixed systems. That said, Fig. 5a indicates that Ti/Sn pairings in the A = Y pyrochlore family do not want to adopt the ordered structure found for GZTO. Thus, the fact that it wants to form a solid solution suggests that other ordered structures might be favorable.

On the other hand, electron diffraction and NMR studies of Sn/Zr pairings in A = Y pyrochlores reveal that there is evidence of a longer-ranged ordering than that of pyrochlore.[27] While those authors were not able to identify the nature of the ordering, our results suggest that this system, at least in the Zr-rich case, would tend to form an ordered structure at low temperature. As always, there is the possibility that another even more stable structure exists for this compound as well.

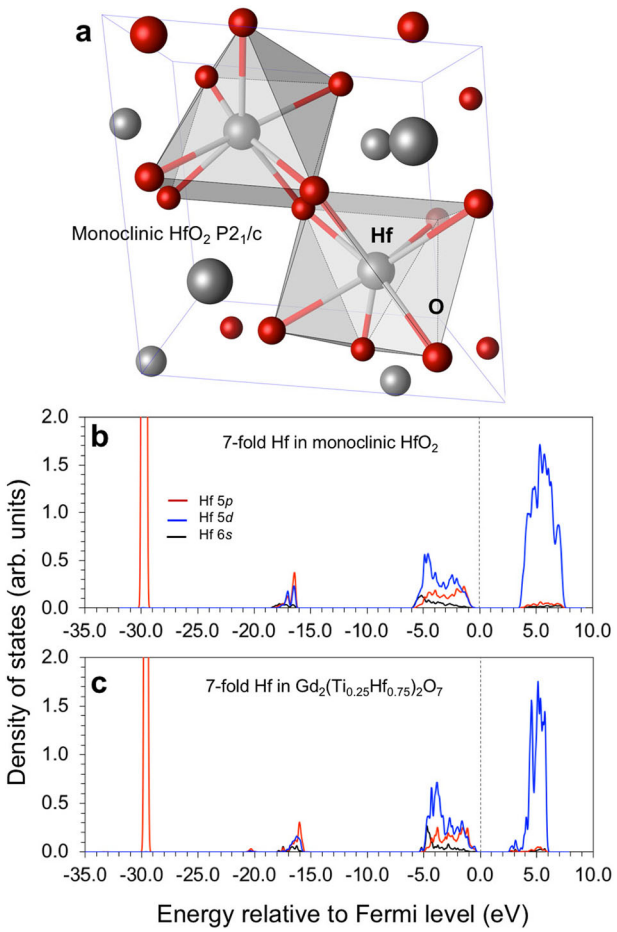

Fig. 6 **a** Polyhedra highlighting a 7-fold coordinated local environment of Hf atoms in ground-state monoclinic structure (space group: $P2_1/c$). For clarity, polyhedra for only two Hf atoms are shown. **b**, **c** Comparison of orbital decomposed partial density of states (DOS) for a 7-fold coordinated Hf atom in HfO_2 and $Gd_2(Ti_{0.25}Hf_{0.75})_2O_7$, respectively

We also note that the double pyrochlore mixing energies for this set of compounds sensitively depend on the nature of the B′ cations (for a given A site chemistry) and the underlying chemical trends can easily be rationalized in terms of relative size and chemical bonding tendencies of the B′ elements. While Ti and Sn cations exhibit relatively smaller ionic radii as B'^{4+} cations and prefer a 6-fold coordinated environment, Zr and Hf possess relatively larger tetravalent ionic radii and have a strong preference for a 7-fold coordinated environment. We note that the chemical propensity for a 7-fold coordination for Hf and Zr is also a reason for the monoclinic ground states of simple oxides of these metals, *i.e.*, HfO_2 and ZrO_2, where the metal ions are 7-fold coordinated. These notions are further illustrated in Fig. 6. While Fig. 6a qualitatively depicts the geometrical similarity of a 7-fold coordination for Hf atom in a double pyrochlore to that in HfO_2, the partial density of states (DOS) for Hf presented in Fig. 6b, quantitatively confirms this by comparing electronic structures of 7-fold coordinated Hf atoms in HfO_2 and $Gd_2(Ti_{0.25}Hf_{0.75})_2O_7$, respectively. Qualitatively similar results are also obtained for the corresponding Zr-based chemistries.

It is also worthwhile to note here that the stabilization achievable through the O relaxations in mixed pyrochlore chemistries is asymmetry with respect to B and B′ cation species. More specifically, for an $A_2(B_{0.25}B'_{0.75})_2O_7$ compound only certain B′ cations can change their coordination from 6-fold to 7-fold as a result of the O relaxations, while all the B cations remain 6-fold

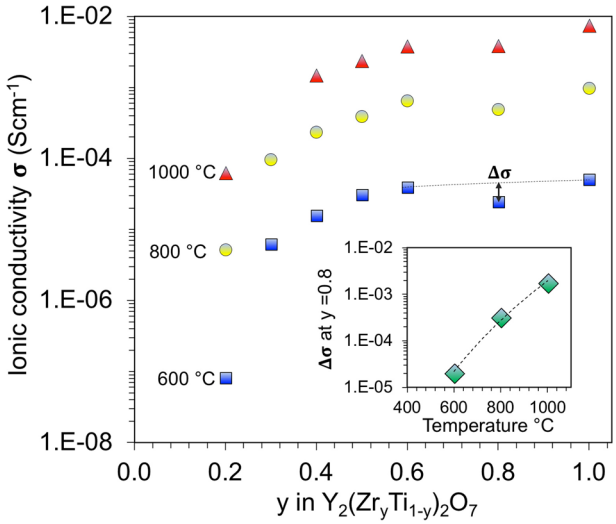

Fig. 7 Experimentally measured ionic conductivity σ for $Y_2(Ti_{1-y}Zr_y)_2O_7$ solid solutions as a function of temperature and Zr content y. Data is replotted from ref. [45]. Inset shows the temperature variation of $\Delta\sigma$, defined as the relative lowering of the ionic conductivity at $y = 0.8$ with respect to a value directly computed by a linear interpolation of the conductivity of the neighboring compositions

coordinated. Therefore, energetic contributions resulting from the O relaxations to the mixing energies (as shown in Fig. 5b) are predominantly governed by the chemical propensity of the B′ cations towards a 7-fold coordination. This implies that for chemistries containing both Hf and Zr on the B-sublattice—such as $A_2(Hf_{0.25}Zr_{0.75})_2O_7$ and $A_2(Zr_{0.25}Hf_{0.75})_2O_7$—the coordination change of the B′ cations (Zr in the former case and Hf in the latter case) is largely responsible for the lowering of the mixing energies.

As a result of the relaxation displacements of the O atom, the compounds with Zr and Hf atoms at the B′ site are not only able to satisfy their natural propensity for a 7-fold B′ coordination, but also the appropriate ionic size of these cation species allows for minimization of the local strains caused as result of the O displacements. This is in contrast to the compounds with Ti and Sn as B′ cations. While both Ti^{4+} and Sn^{4+} ions intrinsically prefer a 6-fold coordination, the much smaller ionic radius of Ti^{4+}, as compared to the Zr^{4+} and Hf^{4+}, further results in energetically unfavorable local strains in case of the O displacements, leading to relatively larger positive energies of mixing in comparison to the corresponding Sn based compounds.

DISCUSSION

These findings have important implications for ionic conductivity in pyrochlores and provide insights into previously observed but yet to be explained trends. For example, Fig. 7 shows experimentally measured ionic conductivities in mixtures of $Y_2Ti_2O_7$ and $Y_2Zr_2O_7$ as a function of both temperature and relative Zr content. Consistent with other studies on mixed $Gd_2Ti_2O_7$ and $Gd_2Zr_2O_7$, the conductivity is relatively low for the pure Ti compound and increases with increasing Zr content y. Most interestingly, however, is that the conductivity is not a monotonic function of y but rather exhibits a small dip at a composition of $y = 0.8$. The size of this dip is temperature dependent. This result suggests that there is some aspect of this composition that is different from the neighboring ones. We suggest that this composition might exhibit an ordered structure of Ti and Zr. Indeed, our DFT calculations indicate that for compositions around $y = 0.75$ the propensity for such ordering is greatest. We cannot rule out that other effects

might be driving this experimental behavior, such as differences in phase separation. Also, the cation mixing in the experimental system may be more complex than we have examined, with mixing between the A and B cations as well. However, it is intriguing that there is some reduction of conductivity at the composition where we predict there to be the greatest ordering. In fact, the presence of 7-fold coordinated Zr would be expected to lead to a reduction of conductivity as it would tend to be a bottleneck for the passage of an oxygen vacancy.

As mentioned in the introduction, mixed pyrochlores have been used as a way of systematically introducing disorder into the compound to examine the effects on ionic conductivity, with conflicting results. Our results suggest that, in addition to introducing two changes to the system at once–a change in chemistry as well as disorder–there may be other effects, such as compositional ordering, that further complicate analysis and comparison. This is also born out by the measurements on mixed $Y_2Ti_2O_7$-$Y_2Zr_2O_7$ discussed above. Thus, there are potential complications to chemical changes that must be considered when interpreting the results from experiments on mixed pyrochlores.

Indeed, changes in Zr coordination, in which Zr goes from a 6-fold to a 7-fold coordination in the pyrochlore matrix, have been observed before in various experimental studies.[28–30] However, in all cases, these changes have been induced by cation mixing and the associated changes in the oxygen distribution. Further, in those studies, any increase in Zr coordination was accompanied by decreases in the coordination of other cations. To the best of our knowledge, our theoretical calculations are the first to demonstrate the stabilization of an ordered structure because of the shift in coordination of Zr.

Finally, our results provide some insight into the fundamental difference in the ionic conductivity in Zr-based pyrochlores as compared to Ti-based compounds. In pyrochlores in which B = Ti, all of the B cations are 6-fold coordinated, as they prefer to be. This essentially locks the oxygen in place, as any movement would disrupt, at least temporarily, the coordination of the Ti cations. However, in the case of B = Zr, the B cations would prefer to have 7-fold coordination. Thus, the system is, in some sense, frustrated. All of the Zr cations would prefer a higher coordination, and that can be achieved at least transiently by shifting oxygen around. This cannot be done for all Zr simultaneously and so leads to a system that is more dynamic than if B = Ti. Thus, the origin of higher conductivity in Zr compounds is not due to a stronger Ti-O bond, but rather a stronger Zr–O interaction that drives the system to constantly shift the oxygen around in a frustrated attempt to increase the Zr coordination. This may lead to longer-range concerted events that drive ionic conductivity in this type of system. Such effects have been proposed earlier by Mohn et al. in the context of ionic conductivity in $Ba_2In_2O_5$.[31]

To conclude, we have found novel low-energy ordered structures for the mixed $Gd_2Ti_2O_7$–$Gd_2Zr_2O_7$ pyrochlores. The lowest energy structures are stabilized by an oxygen relaxation that allows for 7-fold coordination of some of the Zr cations in these structures. This result has implications not only for interpreting experimental results on mixed pyrochlores, but also on the origins of conductivity in these types of systems. Finally, the potential presence of ordered structures in mixed pyrochlores opens a new avenue for tailoring the properties of these systems, in much the same way that is being explored for double perovskites. So-called double pyrochlores extend the functional space of these compounds.

METHODS

DFT calculations were performed using the Vienna *Ab initio* Simulation Package (VASP)[32,33] and employed the Perdew, Burke, and Ernzerhof (PBE)[34] generalized gradient approximation (GGA) exchange-correlation functional. The electronic wave functions were expanded in plane waves up to a cut-off energy of 600 eV. The pseudopotentials based on the projector augmented wave method[35] explicitly included the following valence electronic configurations for different elemental species in $Gd_2(Zr_xTi_{1-x})_2O_7$ chemistries; Gd: $5p^65d^16s^2$, Ti: $3p^63d^2$ $4s^2$, Zr: $4s^24p^64d^25s^2$, and O: $2s^22p^4$. A Gamma-centered automatically-generated $4\times4\times4$ Monkhorst-Pack *k*-point mesh[36] was used for Brillouin-zone integrations for a supercell containing 22 atoms. For larger supercells, the *k*-point meshes were appropriately scaled to give the same *k*-point density in the reciprocal space. Spin-unpolarized calculations were employed at large, however tests with spin-polarized calculations were also performed to confirm both the relative energetics and chemical trends computed with the spin-unpolarized calculations. To obtain a geometry optimized equilibrium structure, atomic positions as well as the supercell lattice parameters were fully relaxed using the conjugate gradient method until all the Hellmann-Feynman forces and the stress component were less than 0.02 eV/Å and 1.0×10^{-2} GPa, respectively.

Table 1. Details of VASP PAW PBE pseudo potentials used in the present study for different elemental species

Elemental species	VASP pseudo potential	Number of included valence electrons
Dy	Dy_3	9
Er	Er_3	9
Gd	Gd_3	9
Hf	Hf_pv	10
Ho	Ho_3	9
La	La	11
Lu	Lu_3	9
Nd	Nd_3	11
O	O	6
Pr	Pr_3	11
Sm	Sm_3	11
Sn	Sn_d	14
Tb	Tb_3	9
Ti	Ti_pv	10
Y	Y_sv	11
Zr	Zr_sv	12

The enumeration of different $Gd_2(Zr_xTi_{1-x})_2O_7$ chemistries and orderings over the parent crystal structure was performed with the CASM software package [https://github.com/prisms-center/CASMcode].[23,37,38] The primitive cells employed for the mixed pyrochlore chemistries contained 22 atoms and configurations spanned by supercells containing up to 66 atoms were enumerated exhaustively. This enumeration resulted in a total of 704 different configurations, for which total energy minimizations and computations were performed within DFT. Different configurations represent different arrangements of Ti and Zr on the B sublattice within the pyrochlore structure. An effort was also made using CASM to construct and parametrize cluster expansion (CE) Hamiltonians in order to perform subsequent finite temperature Monte Carlo simulations.[39–42] However, as discussed further in the results section, large basis deformations encountered during structural relaxations for a subset of $Gd_2(Zr_xTi_{1-x})_2O_7$ chemistries prevented us from fitting CE Hamiltonians reproducing the relative energetics of DFT computations with a high fidelity.

To evaluate the relative tendency of B-site mixing in different pyrochlores as a function of chemistry, mixing energies of 132 "double" pyrochlores (each containing a single A-site and two different B-site cations) were computed. Specifically, the 11 element choices considered for the A-site chemistry were Y, La, Pr, Nd, Sm, Gd, Tb, Dy, Ho, Er and Lu, while the two different elements mixing on the B sub-lattice were selected form a pool of four species, *viz*., Ti, Zr, Sn and Hf. For these elements, the specific choices of the VASP pseudopotentials (along with the associated number of valance electrons) employed in the DFT computations are listed in Table 1. Since an explicit exhaustive enumeration—similar to that for the $Gd_2(Zr_xTi_{1-x})_2O_7$ chemistries described above—for the entire set of 132 double pyrochlores is well beyond the scope of the present work, for practical reasons, we simulated the double pyrochlores in a composition and configuration that resulted in the lowest energy of mixing for the $Gd_2(Zr_xTi_{1-x})_2O_7$ chemistries.

DATA AVAILABILITY

The data that support the findings of this study are available from the corresponding authors upon reasonable request.

ACKNOWLEDGEMENTS

We thank Neil Allan for useful discussions and the group of Richard G. Hennig for help in orthogonalizing the structure used in the simulation of the XRD pattern shown in Fig. 2. BPU and GP were supported by the U.S. Department of Energy, Office of Science, Basic Energy Sciences, Materials Sciences and Engineering Division. The work was performed at the Los Alamos National Laboratory (LANL), an affirmative action equal opportunity employer, operated by Los Alamos National Security, LLC, for the National Nuclear Security Administration of the U.S. DOE under contract DE-AC52-06NA25396. Computational support for this work was provided by LANL's high performance computing clusters.

AUTHOR CONTRIBUTIONS

B.P.U. designed the study. G.P. and B.P.U. performed the high-throughput computations and wrote the manuscript. B.P. helped with CASM computations and analysis of the results. All authors discussed the results and commented on the manuscript.

ADDITIONAL INFORMATION

Supplementary information accompanies the paper on the *npj Computational Materials* website (https://doi.org/10.1038/s41524-018-0144-1).

Competing interests: The authors declare no Competing Interests.

Publisher's note: Springer Nature remains neutral with regard to jurisdictional claims in published maps and institutional affiliations.

REFERENCES

1. Kimble, T., Chou, M. & Chai, B. Scintillation properties of LYSO crystals. *IEEE Nucl. Sci. Symp. Conf. Rec.* **3**, 1434–1437 (2002).
2. Fukushima, T., Stroppa, A., Picozzi, S. & Perez-Mato, J. M. Large ferroelectric polarization in the new double perovskite NaLaMnWO6 induced by non-polar instabilities. *Phys. Chem. Chem. Phys.* **13**, 12186 (2011).
3. Pilania, G. & Uberuaga, B. P. Cation ordering and effect of biaxial strain in double perovskite CsRbCaZnCl. *J. Appl. Phys.* **117**, 114103 (2015).
4. Heitmann, A. A. & Rossetti, G. A. Thermodynamics of ferroelectric solid solutions with morphotropic phase boundaries. *J. Am. Ceram. Soc.* **97**, 1661 (2014).
5. Rost, C. M. et al. Entropy-stabilized oxides. *Nat. Commun.* **6**, 8485 (2015).
6. Suntivich, J., May, K. J., Gasteiger, H. A., Goodenough, J. B. & Shao-Horn, Y. A perovskite oxide optimized for oxygen evolution catalysis from molecular orbital principles. *Science* **334**, 1383 (2011).
7. Vasala, S. & Karppinen, M. A2B'B''O6 perovskites: a review. *Prog. Solid State Chem.* **43**, 1 (2015).
8. Karppinen, M. & Yamauchi, H. In (Ed. Narlikar, A. V.) *Frontiers in Magnetic Materials* 153–184 (Springer-Verlag, Berlin, 2005).
9. King, G. & Woodward, P. M. Cation ordering in perovskites. *J. Mater. Chem.* **20**, 5785 (2010).
10. Davies, P., Wu, H., Borisevich, A., Molodetsky, I. & Farber, L. Crystal chemistry of complex perovskites: new cation-ordered dielectric oxides. *Annu. Rev. Mater. Res.* **38**, 369 (2008).
11. Howard, C. J., Kennedy, B. J. & Woodward, P. M. Ordered double perovskites - a group-theoretical analysis. *IUCr. Acta Crystallogr. Sect. B Struct. Sci.* **59**, 463 (2003).
12. Goodenough, J. B. Electronic and ionic transport properties and other physical aspects of perovskites. *Rep. Progress. Phys.* **67**, 1915 (2004).
13. Uberuaga, B. P. & Pilania, G. Effect of cation ordering on oxygen vacancy diusion pathways in double perovskites. *Chem. Mater.* **27**, 5020 (2015).
14. Serrate, D., Teresa, J. M. D. & Ibarra, M. R. Double perovskites with ferromagnetism above room temperature. *J. Phys. Condens. Matter* **19**, 023201 (2007).
15. Sickafus, K. E. et al. Radiation tolerance of complex oxides. *Science* **289**, 748 (2000).
16. Lang, M. et al. Structural modifications of Gd2Zr2- xTixO7 pyrochlore induced by swift heavy ions: disordering and amorphization. *J. Mater. Res.* **24**, 1322 (2009).
17. Hess, N. J. et al. Spectroscopic investigations of the structural phase transition in Gd2(Ti1-yZry)2O7 pyrochlores. *J. Phys. Chem. B* **106**(18), 4663–4677 (2002).
18. Tuller, H. L. J. Oxygen ion conduction and structural disorder in conductive oxides. *Phys. Chem. Solids* **55**, 1393 (1994).
19. Díaz-Guillén, J. et al. The effect of homovalent A-site substitutions on the ionic conductivity of pyrochloretype Gd2Zr2O7. *J. Power Sources* **186**, 349 (2009).
20. Moreno, K. J. et al. Influence of thermally induced oxygen order on mobile ion dynamics in Gd2(Ti0.65Zr0.35)2O7. *Phys. Rev. B* **75**, 184303 (2007).
21. Reader, S. W. et al. Cation disorder in pyrochlore ceramics: Y MAS NMR and first-principles calculations. *J. Phys. Chem. C.* **113**, 18874 (2009).
22. Fernandes, A. et al. Phase composition and disorder in La (Sn,Ti) O ceramics: new insights from NMR crystallography. *J. Phys. Chem. C.* **120**, 20288 (2016).
23. Thomas, J. C. & der Ven, A. V. Finite-temperature properties of strongly anharmonic and mechanically unstable crystal phases from rst principles. *Phys. Rev. B* **88**, 214111 (2013).
24. Uberuaga, B. P. & Sickafus, K. E. Interpreting oxygen vacancy migration mechanisms in oxides using the layered structure motif. *Comput. Mater. Sci.* **103**, 216 (2015).
25. O'Keeffe, M. & Hyde, B. G. Plane nets in crystal chemistry. *Philos. Trans. R. Soc. A: Math., Phys. Eng. Sci.* **295**, 553 (1980).
26. Slater, J. C. Atomic radii in crystals. *J. Chem. Phys.* **41**, 3199 (1964).
27. de los Reyes, M. et al. The pyrochlore to defect fluorite phase transition in Y2Sn2-xZrxO7. *RSC Adv.* **3**, 5090 (2013).
28. Liu, Y., Withers, R. L. & Noren, L. The pyrochlore to 'defect fluorite' transition in the Y2(ZryTi1−y)2O7 system and its underlying crystal chemistry. *J. Solid State Chem.* **177**, 4404 (2004).
29. Norberg, S. T. et al. Pyrochlore to fluorite transition: the Y2(Ti1−xZrx)2O7 (0.0 ≤ x ≤ 1.0) system. *Chem. Mater.* **24**, 4294 (2012).
30. Zhang, Z. et al. Gradual structural evolution from pyrochlore to defect-fluorite in Y2Sn2−xZrxO7: average vs local structure. *J. Phys. Chem. C.* **117**, 26740 (2013).
31. Mohn, C. E., Allan, N. L., Freeman, C. L., Ravindran, P. & Stølen, S. Order in the disordered state: local structural entities in the fast ion conductor Ba2In2O5. *J. Solid State Chem.* **178**, 346 (2005).
32. Kresse, G. & Furthmüller. Efficient iterative schemes for ab initio total-energy calculations using a planewave basis set. *J. Phys. Rev. B* **54**, 11169 (1996).
33. Kresse, G. & Joubert, D. From ultrasoft pseudopotentials to the projector augmented-wave method. *Phys. Rev. B* **59**, 1758 (1999).
34. Perdew, J. P., Burke, K. & Ernzerhof, M. Generalized gradient approximation made simple. *Phys. Rev. Lett.* **77**, 3865 (1996).
35. Blöchl, P. E. Projector augmented-wave method. *Phys. Rev. B* **50**, 17953 (1994).
36. Monkhorst, H. J. & Pack, J. D. Special points for Brillouin-zone integrations. *Phys. Rev. B* **13**, 5188 (1976).
37. Puchala, B. & Van der Ven, A. Thermodynamics of the Zr-O system from rst-principles calculations. *Phys. Rev. B* **88**, 094108 (2013).
38. Van der Ven, A., Thomas, J., Xu, Q. & Bhattacharya, J. Linking the electronic structure of solids to their thermodynamic and kinetic properties. *Math. Comput. Simul.* **80**, 1393 (2010).
39. Sanchez, J., Ducastelle, F. & Gratias, D. Generalized cluster description of multi-component systems. *Phys. A: Stat. Mech. its Appl.* **128**, 334 (1984).
40. Sanchez, J. M. Cluster expansion and the congurational theory of alloys. *Phys. Rev. B* **81**, 224202 (2010).
41. Asta, M., Wolverton, C., de Fontaine, D. & Dreyssé, H. Effective cluster interactions from cluster-variation formalism. *Phys. Rev. B* **44**, 4907 (1991).
42. Fontaine, D. D. Cluster approach to order-disorder transformations in alloys. *Solid State Phys.* **47**, 33 (1994).
43. Crystal Diffract 6. http://crystalmaker.com/crystaldiffract/.
44. Mathew, K. et al. A materials project based Python tool for high-throughput computational screening of interfacial systems. *Comput. Mater. Sci.* **122**, 183 (2016).
45. Heremans, C., Wuensch, B. J., Stalick, J. K. & Prince, E. Fast-ion conducting Y2 (ZryTi1-y)2O7 pyrochlores: neutron Rietveld analysis of disorder induced by Zr substitution. *J. Solid State Chem.* **117**, 108 (1995).